THE MIXED-PHASE ARCTIC CLOUD EXPERIMENT (M-PACE)

J. Verlinde[1], J.Y. Harrington[1], G.M. McFarquhar[2], V.T. Yannuzzi[1], A. Avramov[1], S. Greenberg[1], N. Johnson[1], G. Zhang[2], M.R. Poellot[3], J.H. Mather[4], D.D. Turner[5], E.W. Eloranta[5], B.D. Zak[6], A.J. Prenni[7], J.S. Daniel[8], G.L. Kok[9], D.C. Tobin[5], R. Holz[5], K. Sassen[10], D. Spangenberg[11], P. Minnis[12], T.P. Tooman[13], M.D. Ivey[6], S.J. Richardson,[1], C.P Bahrmann[1], P.J. DeMott[7], A.J. Heymsfield[14], R. Schofield[8, 15].

[1]The Pennsylvania State University, University Park, Pennsylvania, [2]University of Illinois, Urbana, Illinois, [3]University of North Dakota, Grand Forks, North Dakota, [4]Pacific Northwest National Laboratory, Richland, Washington, [5]University of Wisconsin, Madison, Wisconsin, [6]Sandia National Laboratories, New Mexico, Albuquerque , New Mexico, [7]Colorado State University, Fort Collins, Colorado, [8]NOAA Earth System Research Laboratory, Boulder, Colorado, [9]Droplet Measurement Technologies, Inc, Boulder, Colorado, [10]University of Alaska, Fairbanks, Alaska, [11]Analytical Services & Materials, Inc., Hampton, Virginia, [12]NASA Langley Research Center, Hampton, Virginia, [13]Sandia National Laboratories, California, Livermore, California, [14]National Center for Atmospheric Research, Boulder, Colorado, [15]The Cooperative Institute of Research in Environmental Sciences, University of Colorado – Boulder, Colorado

Corresponding Author: Hans Verlinde, 503 Walker Building, Department of Meteorology, The Pennsylvania State University, University Park, PA 16803. E-mail: verlinde@meteo.psu.edu

Abstract

The Mixed-Phase Arctic Cloud Experiment (M-PACE) was conducted September 27 through October 22, 2004 on the North Slope of Alaska. The primary objective was to collect a data set suitable to study interactions between microphysics, dynamics and radiative transfer in mixed-phase Arctic clouds. Observations taken during the 1997/1998 Surface Heat and Energy Budget of the Arctic (SHEBA) experiment revealed that Arctic clouds frequently consist of one (or more) liquid layers precipitating ice. M-PACE sought to investigate the physical processes of these clouds utilizing two aircraft (an in situ aircraft to characterize the microphysical properties of the clouds and a remote sensing aircraft to constraint the upwelling radiation) over the Department of Energy's Atmospheric Radiation Measurement (ARM) Climate Research Facility (ACRF) on the North Slope of Alaska. The measurements successfully documented the microphysical structure of Arctic mixed-phase clouds, with multiple in situ profiles collected in both single-layer and multi-layer clouds over two ground-based remote sensing sites. Liquid was found in clouds with temperatures down to -30 ^{o}C, the coldest cloud top temperature below -40 ^{o}C sampled by the aircraft. Remote sensing instruments suggest that ice was present in low concentrations, mostly concentrated in precipitation shafts, although there are indications of light ice precipitation present below the optically thick single-layer clouds. The prevalence of liquid down to these low temperatures could potentially be explained by the relatively low measured ice nuclei concentrations.

Capsule: Liquid layers were observed in the Mixed-Phase Arctic Cloud Experiment (M-PACE) at temperatures down to -30^{o}C.

1. Introduction

Significant, interrelated, atmospheric, oceanic and terrestrial changes have been occurring in the Arctic in recent decades (SEARCH SSC, 2001; ACIA 2004). These changes are broad-ranging, impacting every part of the Arctic environment. The Arctic is observed to be warming at a rate approximately twice the global average (ACIA 2004). Climate models appear to have predicted this warming, but the uncertainty in the model projections are larger in the Arctic than over the rest of the globe (Kattsov and Källén 2004). The underlying causes of this enhanced warming and scatter among models in the Arctic are not well understood, but are thought to be related to complex feedback processes unique to the Arctic. Arctic clouds have been identified as playing a central role in several hypothesized feedback processes (Curry et al., 1996). The interactions among clouds, the over- and underlying atmosphere, and the ocean/sea-ice surface are highly complex, arguably the most complex in the Northern Hemisphere. At the same time, these processes and their interactions are less well understood than lower latitude phenomena (Randall et al., 1998; Curry et al., 2000), the result of which is uncertainties in the feedback pathway.

It is well known that Arctic low-level clouds are distinct from their lower latitude counterparts. Weak solar heating, coupled with strong inversions and a combination of sea-ice and ocean for a lower boundary produce clouds with multiple layers and stable temperature profiles (Curry, 1986; Curry et al., 1990, 1996; Randall et al., 1998). Moreover, the recent SHEBA/FIRE-ACE experiments (Uttal et al. 2002; Curry et al. 2000) revealed that mixed-phase clouds appear to dominate the low-cloud fraction within the Arctic during the colder three quarters of the year (Intrieri et al., 2002; Wang et al., 2005). These mixed-phase clouds add complexity to a cloud type that has yet to be well understood. For instance, Arctic low-level mixed-phase clouds tend

to be long-lived, with liquid tops that continually precipitate ice (Pinto 1998; Hobbs and Rangno, 1998; Curry et al., 2000). This longevity is somewhat perplexing given that the Bergeron process should cause rapid glaciation of these clouds (Harrington et al., 1999). While SHEBA/FIRE-ACE enhanced our knowledge of Arctic clouds in general and of mixed-phase clouds in particular, much remains to be learned. For instance, numerical modeling suggests that the ice phase heavily influences cloud evolution (Pinto and Curry, 1995) and that heterogeneous ice nucleation controls mixed-phase longevity (Harrington et al., 1999; Jiang et al., 2000; Morrison et al., 2005). Our poor understanding of the nucleation mechanisms that control ice amounts in Arctic clouds has led to parameterizations that are based more on physical speculation than on observations (Harrington and Olsson, 2001). Nevertheless, such parameterizations are important because the cloud microphysics is intimately tied to cloud-scale dynamics (Harrington et al., 1999) and the underlying surface energy budget (Curry et al., 1997; Walsh and Chapman, 1998; Intrieri et al., 2002). Moreover, the radiative characteristic of these clouds are not fully understood (Pinto et al., 1999).

In order to help bridge the gaps in our understanding of mixed-phase Arctic clouds, the Department of Energy Atmospheric Radiation Measurement Program (DOE-ARM; Stokes and Schwartz, 1994; Ackerman and Stokes, 2003) funded an integrated, systematic observational study. The major objective of the Mixed-Phase Arctic Cloud Experiment (M-PACE), conducted September 27 – October 22, 2004 during the autumnal transition season, was to collect a focused set of observations needed to advance our understanding of the cloud microphysics, cloud dynamics, thermodynamics, radiative properties, and evolution of Arctic mixed-phase clouds.

These data would then be used to improve both detailed models of Arctic clouds and large-scale climate models.

The M-PACE experimental domain (Fig. 1) approximated a single column modeling (SCM) grid-box to facilitate testing of climate model parameterizations in SCMs. This experimental domain is also useful for detailed cloud modeling studies that also require the sorts of large-scale forcing used by SCMs (Jiang et al., 2000). The DOE-ARM North Slope of Alaska (NSA) site at Barrow (http://www.arm.gov/sites/nsa.stm) was supplemented with the High Spectral Resolution Lidar (HSRL; Eloranta, 2005) from the University of Wisconsin and the University of Alaska Fairbanks depolarization lidar (Sassen, 1994). The Pacific Northwest National Laboratory (PNNL) Atmospheric Remote Sensing Laboratory (PARSL; http://www.pnnl.gov/parsl) was deployed at Oliktok Point and was supplemented with a rapid scan Atmospheric Emitted Radiance Interferometer (AERI) from the University of Wisconsin **(**Knuteson et al. 2004). Radiosonde launches were conducted from the four surface sites (Barrow, Atqasuk, Oliktok Point and Toolik Lake) with a maximum of four sondes per day. Two instrumented aircraft participated in the experiment: the University of North Dakota Citation served as an in situ platform, whereas the piloted Scaled Composites Proteus, sponsored by the DOE-ARM Unmanned Aerospace Vehicle program, served as a remote sensing aircraft flying above the cloud decks. In addition to the regular complement of cloud physics probes, the Citation flew a High Volume Precipitation Sampler (HVPS), the Counterflow Virtual Impactor (CVI) from Droplet Measurement Technologies Cloud Spectrometer and Impactor for total water content, and the Colorado State University continuous flow ice thermal diffusion chamber (CFDC).

Together, these measurement systems documented the cloud properties while at the same time providing constraints for radiative transfer calculations above and below the cloud layers.

2. Missions

The Citation and the Proteus flew 13 and 5 missions, respectively, in support of M-PACE. Summaries of the conditions for all flights are provided in Table 1. In total 11 missions were dedicated to characterizing mixed-phase cloud microphysics and 2 flights to cirrus. Ice freezing nuclei (IN) concentrations were measured on all October flights but one. Two flights were dedicated to documenting the IN concentrations in clear skies close to the observed clouds. Cloud top temperatures ranged from -6 to -30 ^{o}C for the St/Sc cases sampled. Droplet concentrations were generally low (~10s cm^{-3}), but two cases exhibited concentrations in the 100s cm^{-3}. Liquid water contents varied between ~0.1 to 1 g m^{-3}. All St/Sc cases had ice precipitation. Figure 2 presents a typical flight pattern for the UND Citation: detailed in situ measurements of cloud properties were obtained by alternate Eulerian and Lagrangian spirals over each of the two ground sites, interspersed by porpoise legs between the two sites to sample the horizontal and vertical variability.

3. Weather Description

The synoptic-scale flow during M-PACE generally controlled the types, extent, and duration of the observed cloud cover. The North Slope of Alaska was under three different synoptic regimes with two transition periods during M-PACE. The first regime (regime I), between Sept. 24 and Oct. 1, was unsettled. A pronounced trough was in place aloft which funneled several short-wave systems into the NSA. During this period the surface was dominated by three small, weak low pressure

systems passing through the area with a large high pressure system northwest of the Alaskan coast over the Arctic Ocean. The first two case days, Sept. 29 and 30, occurred in the heart of this weather regime. September 24-26 was marked by the presence of the first system that moved North along the Canadian/Alaskan border then turned west towards Barrow before dissipating. On Sept. 27, a similar surface low pressure center tracked west out of northern Canada stalling to the south of Barrow with deep clouds. Oliktok Point and Toolik Lake were clear as these regions were located in the dry slot. On Sept. 28, the stalled surface low phase-locked with an upper-level low which caused the surface low to track back eastward, bringing with it the first low-level mixed-phase clouds of the experiment. By Sept. 29 the system was exiting the area, making way for the third system which tracked from west to east through the interior near the Brooks Range during Oct. 1. Overall, this regime was characterized by seasonal to slightly above average temperatures.

October 2-3 marked the transition period between regimes I and II. The upper-level pattern began to change dramatically with the trough breaking down and moving off to the east. In its place a strong, dominant ridge began to build over the Arctic Ocean, remaining in place through Oct. 9. By the 4th of October, synoptic regime II was firmly in place with high pressure building over the pack ice to the northeast of the Alaska coast due to a deepening of cold air over the ice. This strong high dominated the NSA until Oct. 15 and kept several intense storm systems well to the south and west of the NSA. For the majority of the period, flow associated with the high pressure system came out of the east or east-northeast with considerable fetch over the Arctic Ocean before impinging on the Alaska coast. As the high pressure built in over the pack ice a small mid-level low pressure system drifted along the northern Alaska coast from Oct. 5-7 and dissipated between Deadhorse and Barrow on Oct 7. This mid-level low brought a considerable

amount of mid- and upper-level moisture to the NSA and was the source of the cloudiness experienced during the flight operation days of Oct. 5 and 6. By Oct. 8, temperatures over the pack ice had dropped considerably reaching ~-20 C (Fig. 3) with a strengthening of the high. A weak trough moved over the NSA from Oct. 10-13 bringing cooler air to the region. This cooling was also partly due to the advancement of the sea-ice line southward during Oct. 5-10, which allowed air cooled by the pack ice to reach the Alaskan coast (Fig. 3) and, along with it, boundary layer roll clouds (Fig. 4). These rolls likely produced the periodic oscillations (~10 hrs) in cloud depth observed by the MMCR at Barrow and Oliktok Point. This regime was the main driver of cloudiness during the Oct. 8-10 and Oct. 12 case days. Overall, regime II was marked by above average temperatures for the first half of the period (Oct. 4-9) and more seasonal temperatures during the second half (Oct. 10-13) associated with the weak trough. Exceptionally low diurnal temperature ranges were present for the entire period with 9 of 11 days having diurnal ranges of 2°C or less.

Oct. 15-17 marked the transition to Regime III. The surface high over the pack ice slowly drifted southeastward possibly following the deepening of cold air. As the blocking high moved out of the region many systems were able to propagate into the NSA. During the transition, a warm front associated with a low in the Chukchi Sea moved through the area on Oct. 15-16. The block was gone by Oct. 18 ushering in Regime III which lasted for the remainder of the experiment. This period was marked by the influence of a strong and fast developing low pressure center (940 hPa peak strength with a 42 hPa drop analyzed over 24 hours) that formed near Kamchatka and propagated north through the Bering Strait and eventually into the northwestern portion of the Chukchi Sea. The resulting synoptic regime produced southeasterly

flow for much of the NSA (Fig. 5). In addition, patchy ice began to form along the Arctic coastline, particularly east of Barrow. This spawned periods where the NSA was under partially cloudy, or even clear, skies as opposed to the uniform thick boundary layer clouds found throughout regime II. Frontal systems spawned by the low strongly affected the NSA west of a line between Barrow and Oliktok Point, and deep clouds frequently occurred in their presence. Overall regime III was marked by a mean temperature of ~5.5°C above average, the warmest of the three periods. This anomalous warming over most of the NSA resulted from the influence of the warm sector of the intense cyclone spawned off of Kamchatka. For more detailed information concerning weather conditions, cloud data, and forecasts see http://nsa.met.psu.edu.

To provide a more objective classification of weather type during M-PACE, an automated classification procedure, consisting of principal component analysis (PCA) and a two-stage clustering routine, was used (Avramov, 2005). The analysis is applied in two ways. The first categorizes the circulation patterns over Alaska (circulation approach) whereas the second categorizes the atmospheric thermodynamic profiles over Barrow (air-mass approach). The circulation approach is most useful when the evaluation requires details pertaining to atmospheric transport mechanisms, while the air-mass approach is preferred when the categories should be thermodynamically homogeneous (Kalkstein *et al.*, 1996).

When applied to October months for the period 1981 to 2003, the PCA/clustering procedure identified 11 air-mass clusters over Barrow and 11 circulation clusters over Alaska. These clusters or types were then used to categorize the synoptic conditions that took place during M-PACE, the results of which are displayed in Fig. 6. Here colors represent different cluster

classifications, but otherwise have no significance. Regimes II and III were each dominated by the same two circulation patterns, but the thermodynamic profiles over Barrow are quite distinct for the regimes. Stable regimes may be identified where both the profiles and circulation classification remain unchanged for a period of days. The first such period is evident early in Regime II (Oct. 4-7), corresponding to the small low-pressure system over the NSA. The second stable period (Oct. 9-11), after which the NSA progresses through a series of short transition states.

4. Results

A number of outstanding cases were observed during M-PACE. Because a complete overview of all of the cases would be excessive, we instead present results from three cases. These cases are roughly characteristic of the clouds that occurred during M-PACE: a single layer boundary layer stratocumulus case of Oct. 9-11, a cirrus case of Oct. 17 during the second transition (regime II to III) period, and a complicated, multilayer stratus case on Oct. 6 during the first transition (regime I to II).

The 9^{th}-11^{th} was characterized by low-level northeasterly flow off of the pack ice and over the ocean that ultimately reached the NSA. Persistent low-level clouds under a sharp inversion were observed for the entire period, with no mid- or upper-level clouds. Three missions were flown during this period, including a combined Proteus/Citation mission on the 10^{th} to coincide with a close TERRA overpass. Fig. 7 presents PARSL radar/lidar measurements for a 30-minute period centered on the time of a Citation downward spiral. The figure reveals a cloud top increasing from about 1200m to 1300m through the period, while the lidar shows a liquid cloud base at

~800 m (approximately the bottom of the 0-valued depolarization ratio layer). The ceilometer shows the cloud base varying between 800 and 850 m during this period. The radar image suggests that shafts of ice precipitation and/or drizzle (higher reflectivities) were present throughout the cloud layer, while the higher depolarization values below cloud indicate ice precipitation.

The in situ measurements from the Citation downward spiral reveal a similar picture. Fig. 8 shows local cloud base and top slightly below 900 m and just above 1300 m, slightly higher but close to the values observed by the remote sensing instruments. Cloud top values for temperature, liquid water content and mean diameter were -16.9 ^{o}C, 0.36 g m^{-3} and 25 μm, while the droplet number concentration remained approximately constant at 25 cm^{-3} throughout the cloud layer. These values are representative for most flights during this three-day period, with one notable exception: the number concentration varied considerably (20 – 500 cm^{-3}) between days, and even between flights on the same day. From these changes it appears likely that small changes in synoptic flow can produce significant changes in cloud microphysical characteristics, presumably because of changes in the source region of the air. Although some drizzle drops were detected by the 1DC and 2DC probes throughout this period, these were small (typically < 100 μm), so the two-dimensional cloud probe (2DC) numbers may be taken as a proxy for the presence of ice crystals. The approximate ice water content can then be deduced from the 2DC and HVPS data using a mass-diameter relationship calibrated with CVI total water measurements in all-ice conditions. The intermittency of ice in the profile confirms the conclusion drawn from the radar measurements that ice is present in small pockets intercepted occasionally during the spiral.

The imaging and sizing probes provide a view of the particle size distributions and particle types throughout the spiral. Particle size distributions for 30 s flight segments were constructed from the Forward Scattering Spectrometer Probe (FSSP), one- (1DC) and two-dimensional cloud probes, and the High Volume Precipitation Sampler (HVPS). These distributions reveal not only a narrow cloud drop distribution throughout the cloud layer, but also the presence of low concentrations of large precipitation particles (up to 1 cm maximum dimension) all the way up to cloud top (Fig. 9). The Cloud Particle Imager (CPI) reveals the presence of drizzle at cloud top; with some irregular particles being detected at cloud base while images from the HVPS reveal the presence of large irregular ice crystals all the way up to cloud top (Fig. 10).

Surface remote sensing data can provide a detailed look at the processes and properties of Arctic clouds. The analysis potential of the ARM Millimeter Cloud Radar (MMCR) and lidar data is illustrated in Fig. 11. The data presented here are derived from the single layer stratus event but for an earlier period than discussed above. Again, the time-height reflectivity plot in the top panel reveals a precipitating stratus layer consisting of short bursts of higher reflectivity cores, the magnitude of which suggest ice precipitation. Cloud base as indicated by the lidar fluctuates by several hundred meters over the 30-minute period, with a tendency toward lower heights in heavy precipitation. The few cloud base excursions to the surface are likely the results of low-level snow preventing detection of the real base. Tops fluctuate between 1250 m and 1450 m.

The MMCR collected velocity-power spectra during M-PACE, the analysis of which provides further insight into the microphysical characteristics of the layer. The spectrograph (reflectivity

contours in the velocity-height plane) reveals contributions to the total reflectivity from two populations with distinct vertical velocity characteristics. In this spectrograph, the velocity convention is (–) for movement away from the radar, such that precipitation will tend to have (+) velocities, and updrafts (–) velocities. With this knowledge, the two populations may then be identified as non-precipitating and precipitating hydrometeors which are to the left and right, respectively, of the vertical line on the spectrograph. Following the analysis of Shupe et al. (2004), and assuming that the upward moving hydrometeor population is liquid, it is then possible to separate contributions to the total reflectivity from water and ice. This then allows for the calculation of liquid water content (LWC) and vertical velocity (bottom panel). The liquid water contribution to the reflectivity maximizes at -17 dBZ, a value close to the upper range expected for non-precipitating liquid clouds (Frisch et al., 1995). Using the reflectivity – LWC relationship from Shupe et al. (2001), these reflectivity values correspond to LWC values similar to those in Fig. 8, lending confidence that this approach is feasible.

The 17th of October was characterized by mid- and upper-level clouds advecting over the M-PACE domain in advance of a strong front that would pass over Barrow on the 19th of October. The soundings at Barrow revealed a deep moist layer between 500 and 250 hPa with humidity peaking between 505 and 460 hPa. This upper-level moist layer was separated from a lower-level, thin moist layer at 650 hPa by a dry layer. Both the Citation and the Proteus sampled the cloud system. Initially, the Proteus flew over the highest clouds tops, serving as a remote sensing platform, whereas the Citation did spirals through most of the cloud decks. Figure 12 shows a cross section from the Proteus nadir cloud detection lidar from an overpass over the Barrow ARM site and a time-height cross-section from the ARM MMCR reflectivity of the system as it

drifted over. These images reveal a complicated layered cloud structure with multiple, precipitating cirrus layers over a mid-level deck associated with the moisture layer at 500 hPa. The lower panel shows a high resolution image from the University of Alaska Fairbanks lidar of the mid-level cloud layer, revealing a thin (50 m thick) liquid cloud layer consisting of small elements over patchy ice clouds.

The observers in the Citation noted that the sky over Barrow was clear of clouds when they arrived over Barrow at 20:30 UTC, although the lidars detected optically thin cloud layers between 7.5 and 10 km (optical depth $\tau \sim 0.08$ from HRSL) and another layer between 5.5 and 6.3 km ($\tau \sim 0.02$). The Citation did a profile to the west of Barrow through the thicker cloud deck seen on the left-hand side of the Proteus lidar image in Fig. 12a. The in situ measurements from this profile taken at 21:26 GMT (Fig. 13) show a thin liquid cloud layer at 4570 – 4720 m below several layers of cirrus, connected by precipitation, between 7000 – 9100 m. The temperature of this liquid layer was approximately -22 ^{o}C, and the LWC was small at 50 mg m^{-3}. The remote sensing instruments indicate that the Citation did not penetrate through the uppermost cirrus layer. The maximum ice water content (IWC) observed in the cirrus was 60 mg m^{-3}, with bullet rosettes the dominant habit. Mean crystal sizes increased from 100 μm at the cirrus cloud top to 200 μm at the base.

After the Citation departed, the Proteus descended into the upper cirrus layer to perform a closure study with the University of Wisconsin Scanning-HIS instrument on board the Proteus. The scanning – high resolution interferometer sounder (S-HIS) is an aircraft-based version of the ARM AERI that provides accurate measurements of the infrared spectrum at high spectral

resolution. Measurements from this experiment are illustrated in Fig. 14, with AERI measurements of the downwelling radiance at the ground and S-HIS measurements of the upwelling and downwelling radiance within and above cirrus clouds on 17 October 2004. These data are being used to assess capabilities to measure cloud microphysical properties from the interferometers.

On Oct. 6, low-level northeasterly flow and a small, mid-level disturbance combined to produce a complicated multilayer cloud structure over the North Slope (Fig. 15). The highest cloud tops extended to 4.5 km at times (Fig. 15a), although the dominant layer during the period shown had tops between 3.3 and 3.5 km. This dominant layer had significant ice precipitation which produced strong backscatter at radar wavelengths causing the multilayered structure below to be mostly obscured in the radar reflectivity profile (Fig. 15a). However, the narrow beam lidar reveals the complicated layer structure below. Up to 6 liquid cloud layers can be discerned in the lidar depolarization ratio image (Fig. 15b), with individual liquid layers appearing in patches separated by ice precipitation shafts (Fig. 15c). The dominant hydrometeor type map (Fig. 15c) is derived from combined lidar and radar information, through the use of backscatter and depolarization measurements from the HRSL along with reflectivity and vertical velocity measurements from the MMCR (Greenberg, 2005). Individual liquid cloud layers vary from 50 m to 300 m in depth, with optical depths 0.5 to 2 for layers that were penetrated. Interesting, the lidar backscatter between the liquid layers was characteristics of values expected from liquid haze, even while the radar measured reflectivity values of 20 dBZ. Together these measurements suggest that the precipitating ice between the layers consisted of large ice particles of very low

concentration, such that they produce high reflectivities for that larger radar volume, but are missed by the narrow lidar beam.

The in situ measurements from the Citation spiral over Barrow reveal a similar picture. The aircraft was unable to descend into the lowest cloud layer, but did sample several distinct liquid layers (Fig. 16), each of which is capped by a temperature inversion. The profiles of the microphysical properties for most of the layers suggest dynamically quiescent clouds, the exception being the layer at 2600 m where LWC and drop diameter increase linearly with height. At the time of penetration the topmost cloud was experiencing heavy ice precipitation, seen in both the in situ and radar reflectivity profiles (Fig. 15a at 19.15 UTC). The presence of precipitation may explain the irregularities in the microphysical characteristics of the profiles. These characteristics are inconsistent with the radar cloud tops during this period that suggest more active, but small, convection. Indeed, the Citation did measure a vertical velocity pulse of 1.8 m s^{-1} during the profile. The vertical velocity fluctuated between plus and minus 1 m s^{-1} in the second layer, suggesting that this deck, though also precipitating, was experiencing stronger forcing, the origin of which at this stage is not clear. The lower layers are more tenuous, consistent with the picture deduced from the remote sensing instruments of pockets of liquid surviving between ice precipitation shafts.

An additional objective of M-PACE was to provide in situ measurements to evaluate remote sensing measurements. This field experiment provided the opportunity to evaluate two recently developed retrievals for the microphysical properties of mixed-phase clouds from ground-based passive remote sensors. One technique utilizes thermal infrared observations in the 8-13 and 17-

24 m bands observed by the AERI (Turner 2005), while the other observations between 1000-1700 nm (Daniel et al. 2002, 2006). Both techniques take advantage of the changes in the imaginary part of the refractive index of ice relative to liquid water, making observations in wavelength regions where ice and liquid can be spectrally differentiated. The near-infrared spectrometer was deployed at the NSA site from 12 September – 21 Oct.; because it relies on scattering sunlight as its signal, it only makes daytime measurements. Fig. 17 demonstrates the LWP retrieved using the AERI, near-IR spectrometer, and the MWR for a single layer, primarily liquid cloud on 14 September 2004. The agreement between the AERI and near-IR methods is fairly good, while the MWR retrievals are significantly higher for much of the period. A more detailed analysis of this case is given in Daniel et al. (2006).

Moreover, the M-PACE observations are also serving as the basis for the development of new algorithms for satellite identification of mixed-phased cloud. Both aircraft flew several special flight patterns underneath and coincident with satellite overpasses. It should be noted that the definition of what is considered a mixed-phase cloud as seen from a satellite differs from that for ground-based remote sensing because of the big differences in sampling volume. In the context of satellite observations, a mixed-phase cloud is defined to be where ice and liquid co-exists in the same satellite sampling volume or, alternatively, where ice and liquid are found in stratified layers within the satellite footprint. One new algorithm uses the infrared channels of the MODerate-resolution Imaging Spectroradiometer (MODIS), and has the advantage that it can be applied equally well to day and night time scenes (Spangenberg et al., 2006). Successful implementation of this algorithm will extend current abilities to detect mixed-phase clouds

systems over the Arctic and will allow for a better understanding of their spatial extent and relationship to synoptic-scale weather systems.

This new technique is illustrated on MODIS data taken 22:10 UTC on 8 Oct 2004. The 11μm brightness temperature (Fig. 18a) image shows a stratus cloud with values ranging from 255-265 K. Most of the cloud systems are mixed with supercooled liquid tending to be found in areas where the 11μm brightness temperatures values are somewhat higher. The brightness temperature difference between 8.5 and 11μm (Fig. 18b) is a general indicator of the relative amount of liquid at the top of mixed-phase clouds with lower values indicating more liquid (Fig. 18c). The surface remote sensors indicated mixed phase cloud over Barrow at the Terra overpass time is mixed, in general agreement with the MODIS phase retrieval. An hour long segment of the Citation's flight track centered at the Terra overpass time is shown on the MODIS phase image. The corresponding altitude and in situ phase determinations for this segment are plotted in Fig 18d. The in situ liquid and ice water content measurements were combined to obtain the relative amount of liquid along the flight path. These time series data reveal a similar picture of the phase composition of clouds deduced from other days, showing many changeovers from liquid (Rliq > 90%) to ice (Rliq < 10%) dominated samples, with a few regions containing more balanced mixtures of liquid and ice, consistent with the satellite definition of mixed phase clouds.

5. Summary

The Mixed-Phase Arctic Cloud Experiment successfully documented the microphysical structure of Arctic mixed-phase clouds, with multiple in situ profiles collected in both single-layer and

multi-layer clouds over the two ground-based remote sensing sites at Barrow and Oliktok Point. Liquid was found in clouds with temperatures down to -30 ^{o}C, the coldest cloud top temperature below -40 ^{o}C sampled by the aircraft. The remote sensing instruments suggest that ice was present in low concentrations, mostly concentrated in precipitation shafts, although there are indications of light ice precipitation present below the optically thick single-layer clouds. The prevalence of liquid down to these low temperatures could potentially be explained by the relatively low ice nuclei measured (Prenni et al. 2006; Fig. 19). Flights into Arctic cirrus clouds revealed microphysics properties very similar to their mid-latitude in situ formed cousins, with dominant ice crystal habit bullet rosettes. Data from all these flights are freely available for all research purposes (after registration at the same site), and can be found at http://iop.archive.arm.gov/ under IOP data/2004/nsa/mpace.

Acknowledgements: We would like to acknowledge all the people who endured difficult conditions in the field to collect these data. We thank Richard Flanders of the University of Alaska Fairbanks for hosting us at the NSF LTER site at Toolik Lake, the staff of the Oliktok Point Defense Early Warning site for hosting PARSL, Dr. Peter Q. Olsson and his staff at the Alaska Experimental Forecast Facility, University of Alaska Anchorage for their help with the RAMS forecast model, and the staff of the DOE-ARM NSA operations for hosting (and protecting) personnel at Barrow and Atqasuk. This research was supported by the Office of Biological and Environmental Research of the U.S. Department of Energy as part of the Atmospheric Radiation Measurement and Atmospheric Radiation Measurement Unmanned Aerial Vehicle programs.

References

Ackerman, T.P. and Stokes, G.M., 2003: The Atmospheric Radiation Measurement Program. *Physics Today,* **56,** 38-44.

ACIA, 2004: *Impacts of a warming Arctic: Arctic climate impact assessment.* http://www.acia.uaf.edu, 139 pp.

Curry, J. A., 1986: Interactions among Turbulence, Radiation and Microphysics in Arctic Stratus Clouds. *J. Atmos. Sci.*, **43**, 90-106.

Curry, J.A., F.G. Meyer, L.F. Radke, C. Brock, and E.E. Ebert, 1990: Occurrence and characteristics of lower tropospheric ice crystals in the Arctic, *J. Climate*, **10**, 749-764.

Curry, J.A., W.B. Rossow, D.A. Randall and J.L. Schramm. 1996: Overview of Arctic cloud and radiation characteristics**.** *J. Climate*, **9**,1731–1764.

Curry, J. A., J. O. Pinto, T. Benner and M. Tschudi, 1997: Evolution of the cloudy boundary layer during the autumnal freezing of the Beaufort Sea. *J. Geophys. Res*., **102 (D12)**, 13851-13860.

Curry, J.A. and Co-Authors, 2000: FIRE Arctic clouds experiment. *Bull. Amer. Meteor. Soc.,* **81**, 5-29.

Daniel, J.S., S. Solomon, R.W. Portmann, A.O. Langford, C.S. Eubank, E.G. Dutton and W. Madsen, Cloud liquid water and ice measurements from spectrally resolved near-infrared observations: A new technique, J. Geophys. Res., **107**, 4599, doi:10.1029/2001JD000688, 2002.

Daniel, J. S., Portmann, R. W., Miller, H. L., Solomon, S., Langford, A. O., Eubank, C. S., Schofield, R., Turner, D. D., Shupe, M. D., Cloud property estimates from zenith spectral measurements of scattered sunlight between 0.9 and 1.7 mm, submitted to Journal of Geophysical Research, 2006.

Eloranta, E. W., 2005: High Spectral Resolution Lidar. *Lidar: Range-Resolved Optical Remote Sensing of the Atmosphere*, Klaus Weitkamp Ed, Springer Series in Optical Sciences, Springer-Verlag, 460 pp.

Frisch, A.S., C.W. Fairall, J.B. Snider, 1995: Measurement of Stratus Cloud and Drizzle Parameters in ASTEX with a K_{α}-Band Doppler Radar and a Microwave Radiometer *J. Atmos. Sci.*, **52**, 2788-2799.

Greenberg, S.D, 2005: *Objective Arctic cloud phase determination.* M.S. Thesis, Dept. of Meteorology, The Pennsylvania State University, University Park, PA 16803.

Harrington, J.Y. and P.Q. Olsson, 2001: A method for the parameterization of cloud optical properties in bulk and bin microphysical models. Implications for Arctic cloudy boundary layers. *Atmos. Res*. **57**, 51-80.

Harrington, J.Y, T. Reisin, W.R. Cotton, and S.M. Kreindenweis, 1999: Cloud resolving simulation of Arctic stratus. Part II: Transition season clouds, *Atmos. Res*. **51**, 45-75.

Herman, G. and J.A. Curry, 1984: Observational and theoretical studies of solar radiation in Arctic clouds. *J. Climate Appl. Meteor*., **23**, 5-24.

Hobbs, P.V and A. L. Rangno, 1998: Microstructures of low and middle-level clouds over the Beaufort Sea, *Quart. J. Roy. Meteor. Soc.*, **24**, 2035-2071.

Intrieri, J.M., M.D. Shupe, T. Uttal, and B.J. McCarty, 2002: An annual cycle of Arctic cloud characteristics observed by radar and lidar at SHEBA. *J. Geophys. Res*., **107 (C10),** 10.1029/2000JC000423.

Intrieri, J.M., C.W. Fairall, M.D. Shupe, P.O.G. Persson, E.L. Andreas, P.S. Guest, and R.E. Moritz, 2002: An annual cycle of Arctic surface cloud forcing at SHEBA, *J. Geophys. Res*., **107 (C10),** 8039, 10.1029/2000JC000439.

Jiang, H., W.R. Cotton, J.O. Pinto, J.A. Curry, and M.J. Weissbluth, 2000: Cloud resolving simulations of mixed-phase Arctic stratus observed during BASE: Sensitivity to concentration of ice crystals and large-scale heat and moisture advection. *J. Atmos. Sci*., **57**, 2105-2117.

Kattsov, V. M., and E. Källén, 2004: Modeling and scenarios for the Arctic. In: *Impacts of a warming Arctic, Arctic Climate Impacts Assessment* [J. S. Hassol], available from http://www.acia.uaf.edu.

Kalkstein, L.S., M.C. Nichols, C.D. Barthel, and J.S. Greene, 1996: A new spatial synoptic classification: application to air-mass analysis. Int. J. Clim., 16, 983-1004.

Khvorostyanov, V.I., J,A. Curry, I. Gultepe, and K. Strawbridge, 2003: A springtime cloud over the Beaufort Sea polynya: Three-dimensional simulation with explicit spectral microphysics and comparison with observations. *J. Geophys Res*., **108 (D9)**, 4296, 10.1029/2001JD001489.

Knuteson, R. O. and Co-Authors, 2004: Atmospheric Emitted Radiance Interferometer. Part I: Instrument Design. *J. Atmos. Oceanic Technol.* **21**, 1763-1776.

McFarquhar and Co-Authors, 2005: Assessing Current Parameterizations of Mixed-phase Clouds Using In-Situ Profiles Measured During the Mixed-Phase Cloud Experiment. 15th ARM Science Team Mtg., Daytona Beach, FL. (Available at http://www.arm.gov/publications/proceedings/conf15/extended_abs/mcfarquhar_gm3.pdf)

Morrison, H., M. D. Shupe, J. O. Pinto, J. A. Curry, 2005: Possible roles of ice nucleation mode and ice nuclei depletion in the extended lifetime of Arctic mixed-phase clouds. *Geophys. Res. Lett.*, **32**, L18801, 10.1029/2005GL023614.

Pinto, J.O., 1998: Autumnal mixed-phase cloudy boundary layers in the Arctic. *J. Atmos. Sci.*, **55**, 2016-2038.

Pinto, J.O. and J.A. Curry, 1995: Atmospheric convective plumes emanating from leads, 1. Microphysical and radiative processes. *J. Geophys. Res*., **100**, 4633-4642.

Pinto, J.O, J.A. Curry, and A.H. Lynch, 1999: Modeling clouds and radiation for the November 1997 period of SHEBA using a column climate model. *J. Geophys. Res*., **104 (D6),** 6661-6678.

Prenni, A.J. and CO-Authors, 2006: Do Aerosols Regulate Arctic Cloudiness? *Bull. Amer. Meteor. Soc., Submitted.*

Randall, D.A. and Co-Authors, 1998: Status of and Outlook for Large-Scale Modeling of Atmosphere–Ice–Ocean Interactions in the Arctic. *Bull. Amer. Meteor. Soc.*, **79**, 197–219.

Sassen, K., 1994: Advances in polarization diversity lidar for cloud remote sensing. *Proc. IEEE, Remote Sensing Instruments for Environmental Research*, **82**, 1907-1914.

SEARCH SSC, 2001: *SEARCH: Study of Environmental Acrctic Change, Science Plan,* 2001, Available from: Polar Science Center, Applied Physics Laboratory, University of Washington, Seattle, 89 pp.

Shupe, M. D., T. Uttal, S.Y. Matrosov and A.S. Frisch, 2001: Cloud water contents and hydrometeor sizes during the FIRE Arctic Clouds Experiment. *J. Geophys. Res*., **106 (D14),** 15,015 – 15,028.

Shupe, M. D., P. Kollias, S.Y. Matrosov and T.L. Schneider, 2004: Deriving Mixed-Phase Cloud Properties from Doppler Radar Spectra. *J. of Atmos. Oceanic Technol.,* **21**, 660–670.

Spangenberg, D. A., P. Minnis, M. D. Shupe, and M. R. Poellot, 2006: Retrieval of cloud phase over the Arctic using MODIS 6.7 - 12 μm data. *Proc. AMS 14th Conf. Satellite Meteorol. and Oceanog.,* Atlanta, GA, 29 Jan. - 2 Feb., CD-ROM, 8.2.

Stokes, G.M. and S.E. Schwartz, 1994: The Atmospheric Radiation Measurement (ARM) Program: programmatic background and design of the cloud and radiation test bed. *Bull. Amer. Meteor. Soc.*, **75**, 1201-1221.

Turner, D.D., 2005: Arctic mixed-phase cloud properties from AERI-lidar observations: Algorithm and results from SHEBA. J. Appl. Meteor., 44, 427-444.

Uttal, T., and Co-Authers, 2002: Surface Heat Budget of the Arctic Ocean. *Bull. Amer. Meteor. Soc.,* **83**, 255–275.

Walsh, J.E. and W.L. Chapman, 1998: Arctic cloud-radiation-temperature associations in observed data and atmospheric reanalyses. *J. Climate*, **11**, 3030-3045.

Wang, Z., K. Sassen, D. Whiteman, and B. Demoz, 2005: Arctic mixed-phased cloud microphysical properties retrieved from ground-based active and passive remote sensors. *Proc. AMS 8th Conf. on Polar Meteorology and Oceanography*, paper 6.3, San Diego, CA.

Figure and Table Captions

Figure 1: M-PACE experimental domain on the North Slope of Alaska. The operation center was located in Prudhoe Bay, south-east of Oliktok Point.

Figure 2: Flight pattern of the UND Citation for the October 6 flight. The locations of the two primary ground-base remote sensing sites (Barrow and Atqasuk) are indicated.

Figure 3: ETA analysis for 1200UTC Saturday 9 October 2004. Shown are temperatures (shaded), mean sea level pressure (contoured) and wind (barbs).

Figure 4: MODIS visible image of the Arctic Ocean and Northern Alaska 9 October 2004.

Figure 3: ETA analysis for 1200UTC Wednesday 20 October 2004. Shown are temperatures (shaded), mean sea level pressure (contoured) and wind (barbs).

Figure 4: Objective classification of October M-PACE case-days. Each color represents a different cluster. The upper bar show clusters of similar thermodynamic profiles (Wx) over Barrow, while the lower bar shows synoptic circulation clusters.

Figure 5: PARSL radar reflectivity (top), lidar backscatter (middle) and depolarization (bottom) for the UND Citation over flight on 10 October 2004.

Figure 6: UND Citation *in situ* measurements from a single spiral over Oliktok point, 21:45 UTC 10 October 2004, corresponding to the PARSL observations in Fig. 7. a) Temperature, b) liquid (measured and calculated adiabatic) and total water content from the King probe (black), calculated (blue), and CVI (red), C) mean diameter from the FSSP, and d) number concentration from the FSSP (black) and 2-DC probes.

Figure 7: Example 30-s averaged size distributions measured on October 10, 2004 between 2140 and 2147 GMT for the same profile shown in Figure 8. The distributions are derived from FSSP, 1- and 2-DC and HVPS probes (see McFarquhar et al., 2005).

Figure 8: Examples of selected CPI and HVPS images measured on October 10, 2004 between 2140 and 2147 GMT for the same profile shown in Figures 8 and 9. The smaller spherical images near cloud top (CPI) are small drizzle or supercooled drops. Larger ice crystal images show dominance of irregular and rimed crystal shapes. Even though the largest crystals measured by HVPS are more frequent near and below cloud base, they can occur throughout depth of cloud (see McFarquhar et al. 2005).

Figure 9: MMCR analysis for a single profile, 02:06 UTC 9 October 2004. The top panel shows the MMCR reflectivity and lidar detected cloud base, the middle panel an MMCR spectrograph, and the lower panel retrieved profiles from the spectrograph analysis. The bold dashed lines represent the reflectivity attributed to the liquid (red) and ice (blue) particles in the cloud, while profiles of retrieved liquid water content (blue) and vertical velocity (red) are indicated by the thin solid lines.

Figure 10: Proteus nadir Cloud Detection Lidar range-corrected backscatter, ARM MMCR reflectivity, and University of Alaska Depolarization Lidar backscatter of the cirrus case day, 17 October 2004.

Figure 11: Same as Figure 8, but for 21:26 UTC 17 October 2004.

Figure 12: Ground-based AERI-ER and Scanning-HIS measurements (up and down from a 9 and 12 km flight altitude) at Barrow, AK on 17 October 2004 during the M-PACE experiment. The cloud boundary inset is based on onboard lidar backscatter data.

Figure 13: MMCR radar reflectivity (top) and radar/lidar cloud phase mask (middle) for the UND Citation flight over Barrow on 6 October 2004.

Figure 14: Ground-based AERI-ER and Scanning-HIS measurements (up and down from a 9 and 12 km flight altitude) at Barrow, AK on 17 October 2004. The cloud boundary inset is based on the Proteus cloud detection lidar backscatter data.

Figure 15: a) MMCR radar reflectivity (top), b) lidar backscatter (middle) and c) radar/lidar cloud phase mask for the UND Citation flight over Barrow on 6 October 2004.

Figure 16: Same as Figure 8, but for 6 October 2004.

Figure 17: Comparison between three liquid water content retrieval algorithms relying on different parts of the electromagnetic spectrum: microwaves (red line, MWR), infrared bands (blue, AERI) and near-infrared bands (black, near infrared spectrometer).

Figure 18: Terra-MODIS imagery and in-situ cloud phase determination from the UND Citation for 22:10 UTC 8 Oct 2004. (a) 11 μm brightness temperature, (b) brightness temperature difference between 8.5 and 11 μm, (c) cloud phase mask, with Citation flight track and surface based phase retrieval, and (d) Citation cloud phase. The surface-based phase retrieval and CIT flight track are also plotted in (c). The LIQ and SLIQ terms in (c) represent liquid and supercooled liquid water, respectively.

Figure 19: Ice nuclei concentration (60 s average, and corrected to STP) as a function of CFDC processing temperature. Data are limited to measurements for which processing humidity was greater than water saturation, in order to capture deposition, immersion, and condensation freezing nuclei. Individual flights are delineated by symbol. IN concentrations plotted at 0.001 L^{-1} were below background levels, and constituted 85% of

the measurements. Thus, while many of the IN measurements shown fall between 1 L^{-1} and 10 L^{-1}, project average IN concentrations were generally below 1 L^{-1}.

Table 1: Summary of M-PACE aircraft operations. Proteus flight days are indicated with *, satellite coordination with $^{\&}$.

Date	**Category**	**T_{min}(C)**	**FSSP (cm^{-3})**
09/29	BL St	-15	70-90
09/30	Multi-layer St	-15.5	20-70
10/05	Multi-layer St	-6	100-400
10/06	Multi-layer St	-17	25-50
10/08*&	Multi-layer St	-11	20-30
10/09a*	BL St	-16	50-100
10/09b	BL St	-15	300-500
10/10*&	BL St	-17	20-40
10/12*&	BL St	-15	40-60
10/17*&	Ci	-57	50 L^{-1} 2DC
10/18	Ci	-55	20 L^{-1} 2DC
10/20	Aerosol/Sc	-13.5	10-30
10/21	Aerosol/Sc	-23/-30	15

Figure 1: M-PACE experimental domain on the North Slope of Alaska. The operation center was located in Prudhoe Bay, south-east of Oliktok Point.

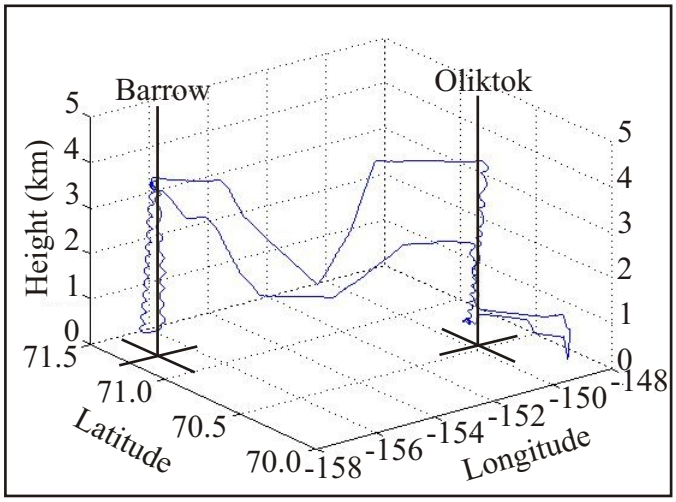

Figure 2: Flight pattern of the UND Citation for the October 6 flight. The locations of the two primary ground-base remote sensing sites (Barrow and Atqasuk) are indicated.

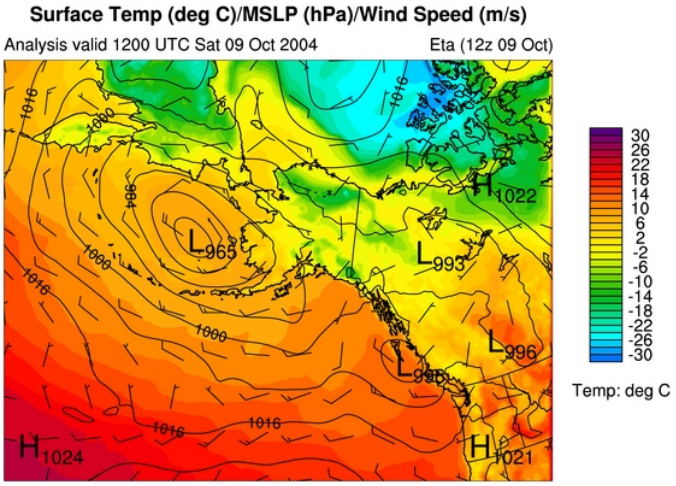

Figure 3: ETA analysis for 1200UTC Saturday 9 October 2004. Shown are temperatures (shaded), mean sea level pressure (contoured) and wind (barbs).

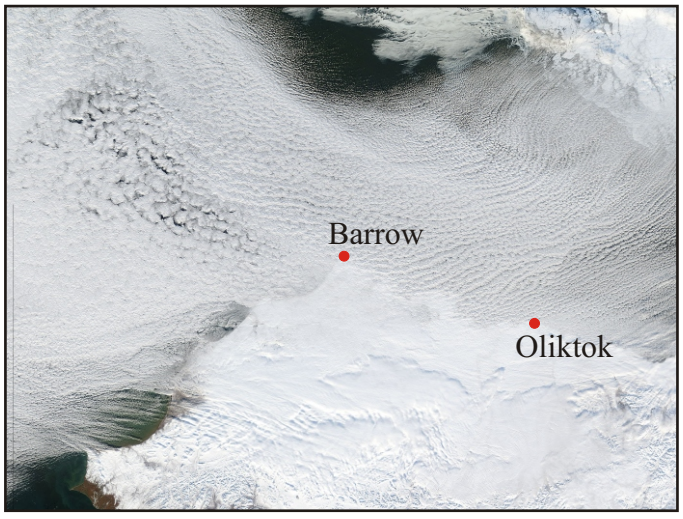

Figure 4: MODIS visible image of the Arctic Ocean and Northern Alaska 9 October 2004

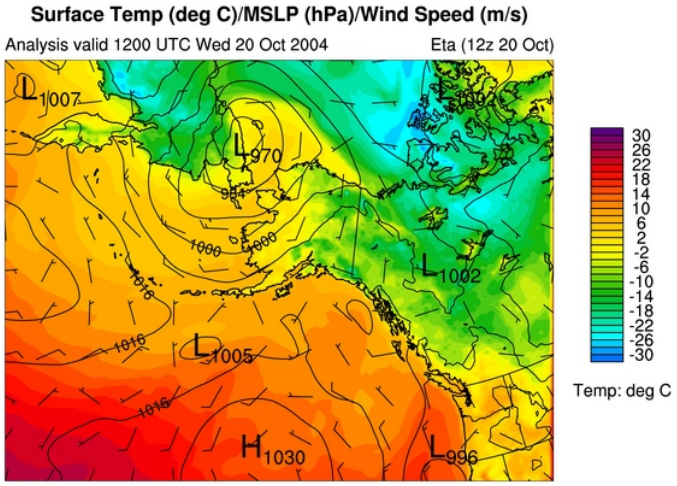

Figure 5: ETA analysis for 1200UTC Wednesday 20 October 2004. Shown are temperatures (shaded), mean sea level pressure (contoured) and wind (barbs)

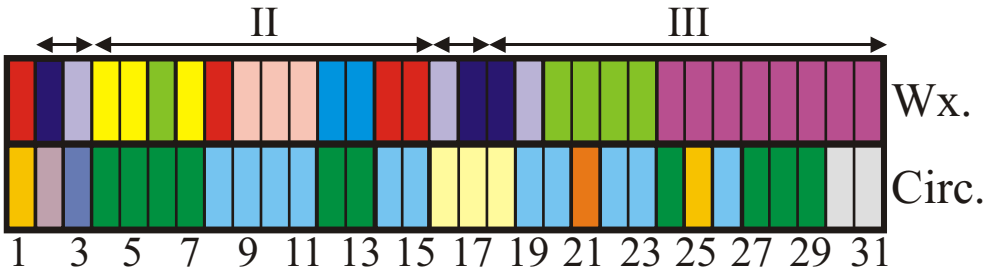

Figure 6: Objective classification of October M-PACE case-days. Each color represents a different cluster. The upper bar show clusters of similar thermodynamic profiles over Barrow, while the lower bar shows synoptic circulation clusters.

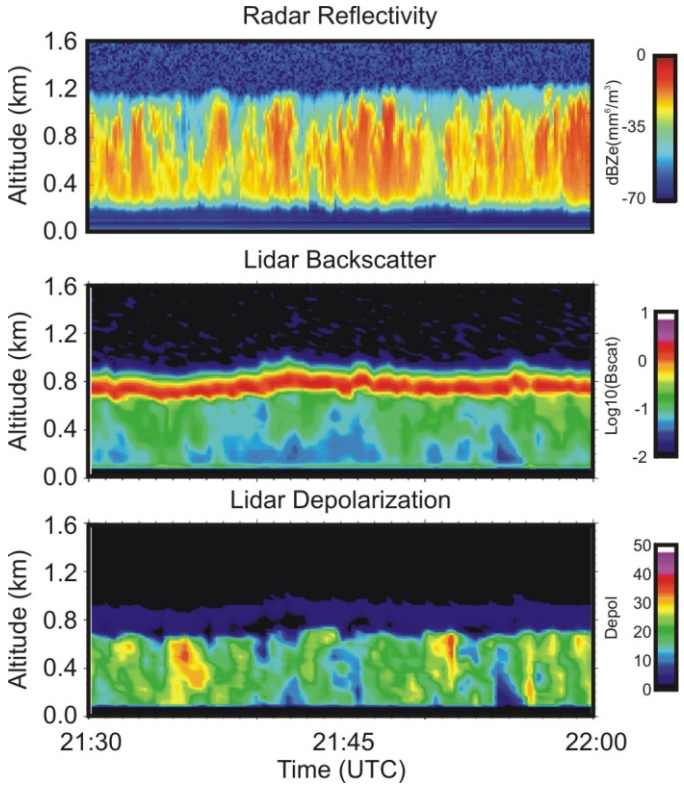

Figure 7: PARSL radar reflectivity (top), lidar backscatter (middle) and depolarization (bottom) for the UND Citation over-flight on 10 October 2004.

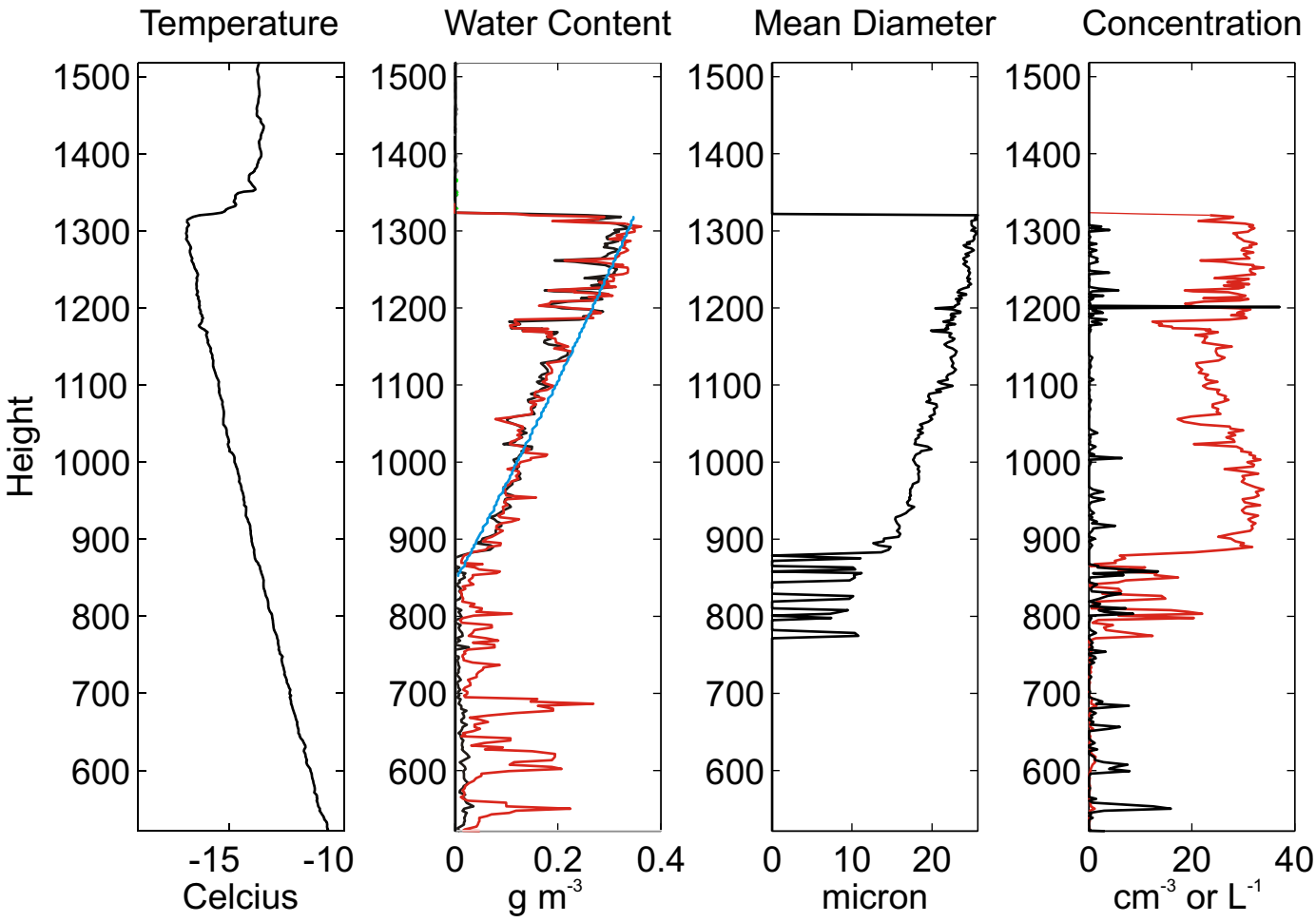

Figure 8: UND Citation in situ measurements from a single spiral over Oliktok point, 21:45 UTC 10 October 2004, corresponding to the PARSL observations in Fig. 7. a) Temperature, b) liquid (measured and calculated adiabatic) and total water content from the King probe (black), calculated (blue), and CVI (red), C) mean diameter from the FSSP, and d) number concentration from the FSSP (cm^{-3}; black) and 2-DC (L^{-1}) probes.

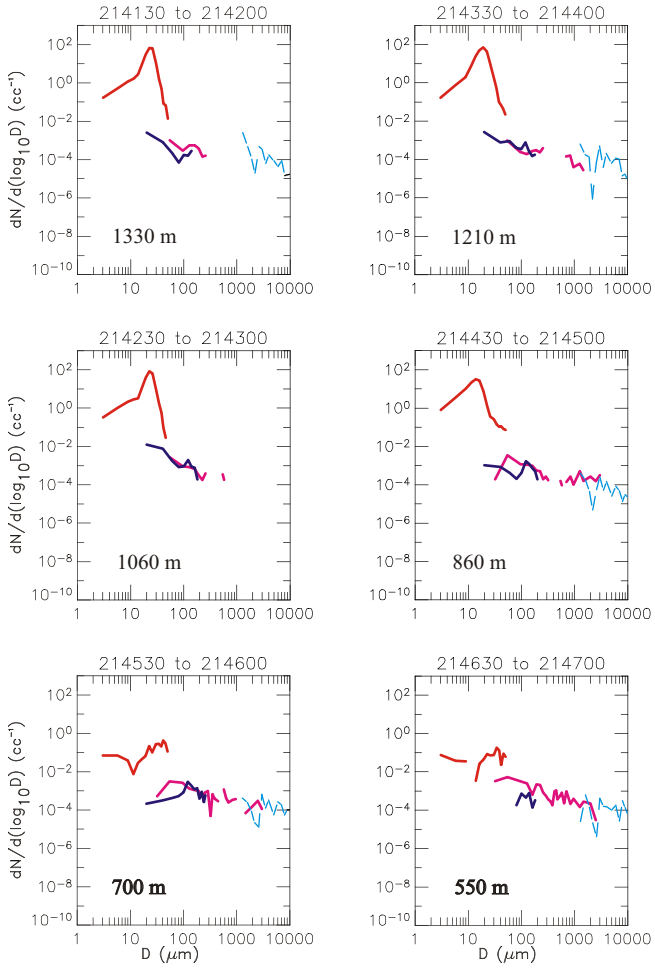

Figure 9: Example 30-s averaged size distributions measured on October 10, 2004 between 2140 and 2147 GMT for the same profile shown in Fig. 8. The distributions are derived from FSSP, 1- and 2-DC and HVPS probes (see McFarquhar et al., 2005).

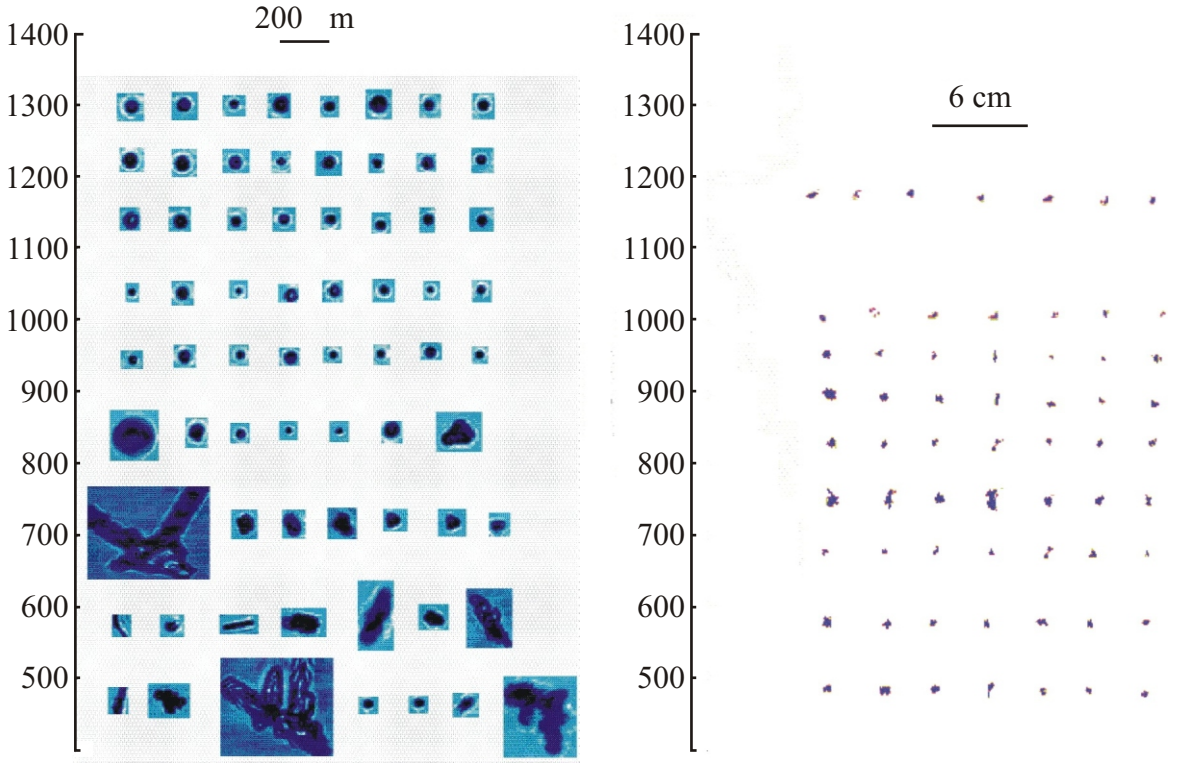

Figure 10: Examples of selected CPI and HVPS images measured on October 10, 2004 between 2140 and 2147 GMT for the same profile shown in Figures 8 and 9. The smaller spherical images near cloud top (CPI) are small drizzle or supercooled drops. Larger ice crystal images show dominance of irregular and rimed crystal shapes. Even though the largest crystals measured by HVPS are more frequent near and below cloud base, they can occur throughout depth of cloud (see McFarquhar et al. 2005).

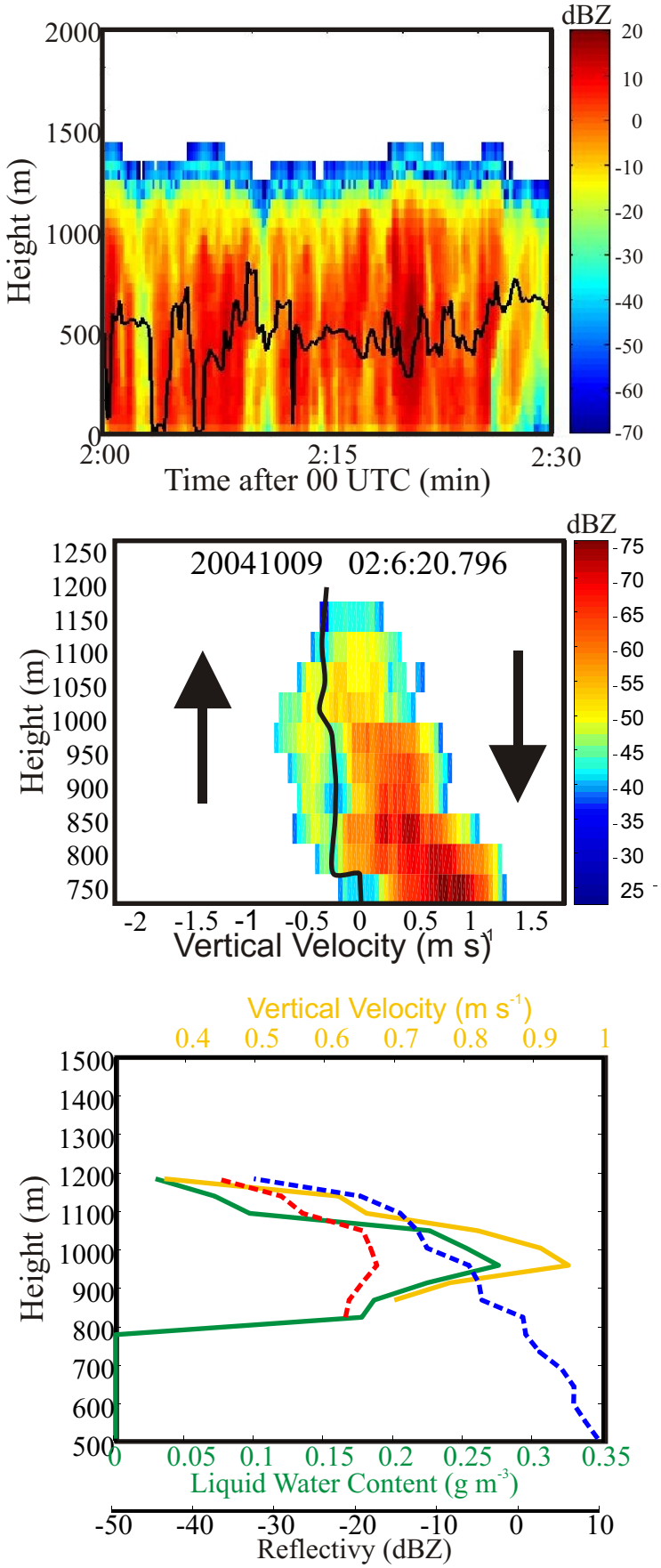

Figure 11: MMCR analysis for a single profile, 02:06 UTC 9 October 2004. The top panel shows the MMCR reflectivity and lidar detected cloud base, the middle panel an MMCR spectrograph, and the lower panel retrieved profiles from the spectrograph analysis. The dashed lines represent the reflectivity attributed to the liquid (red) and ice (blue) particles in the cloud, while profiles of retrieved liquid water content (green) and vertical velocity (gold) are indicated by the solid lines.

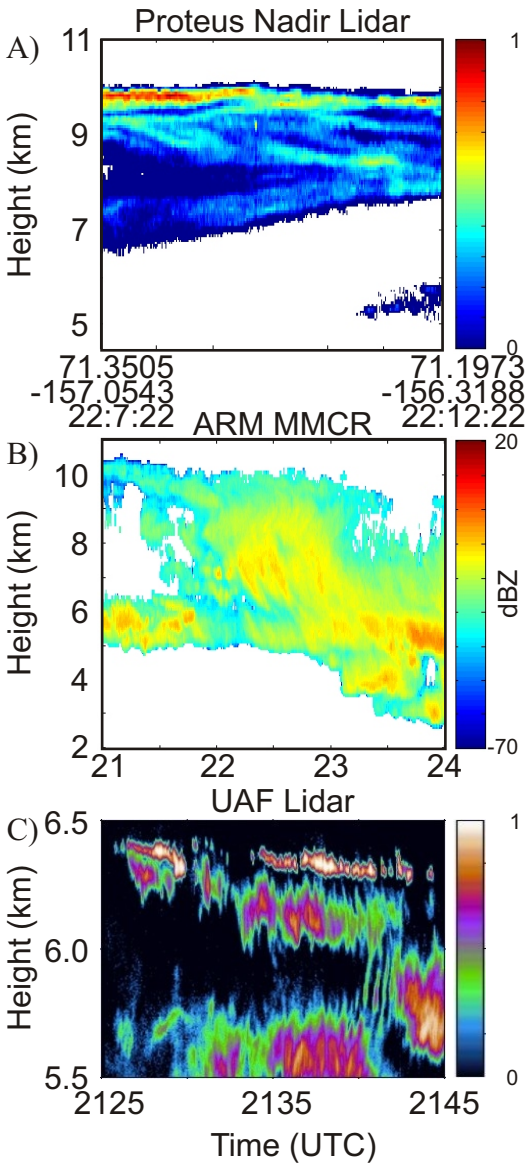

Figure 12: Proteus nadir Cloud Detection Lidar range-corrected backscatter, ARM MMCR reflectivity, and University of Alaska Depolarization Lidar backscatter of the cirrus case day, 17 October 2004.

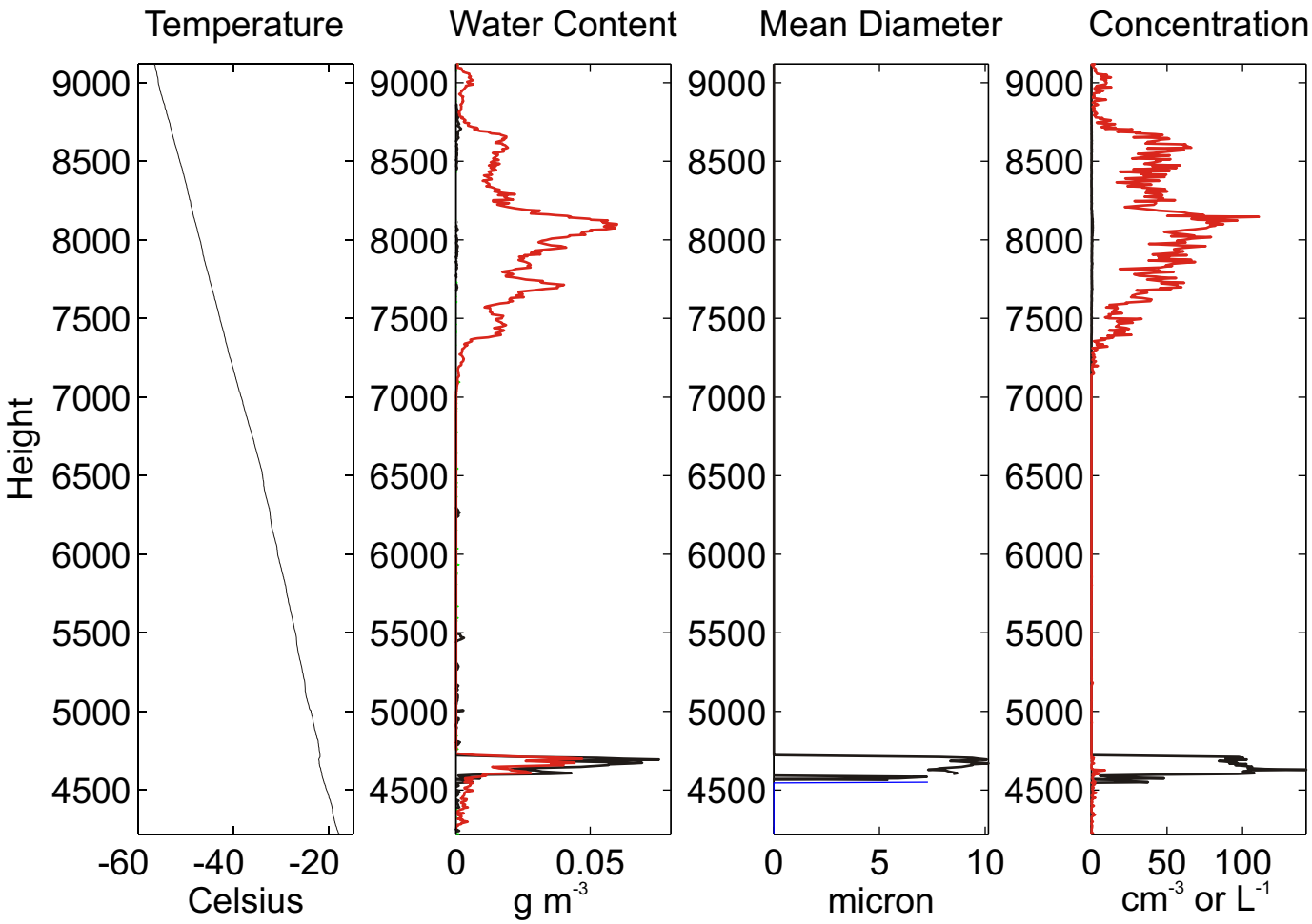

Figure 13: Same as Figure 8, but for 21:26 UTC 17 October 2004.

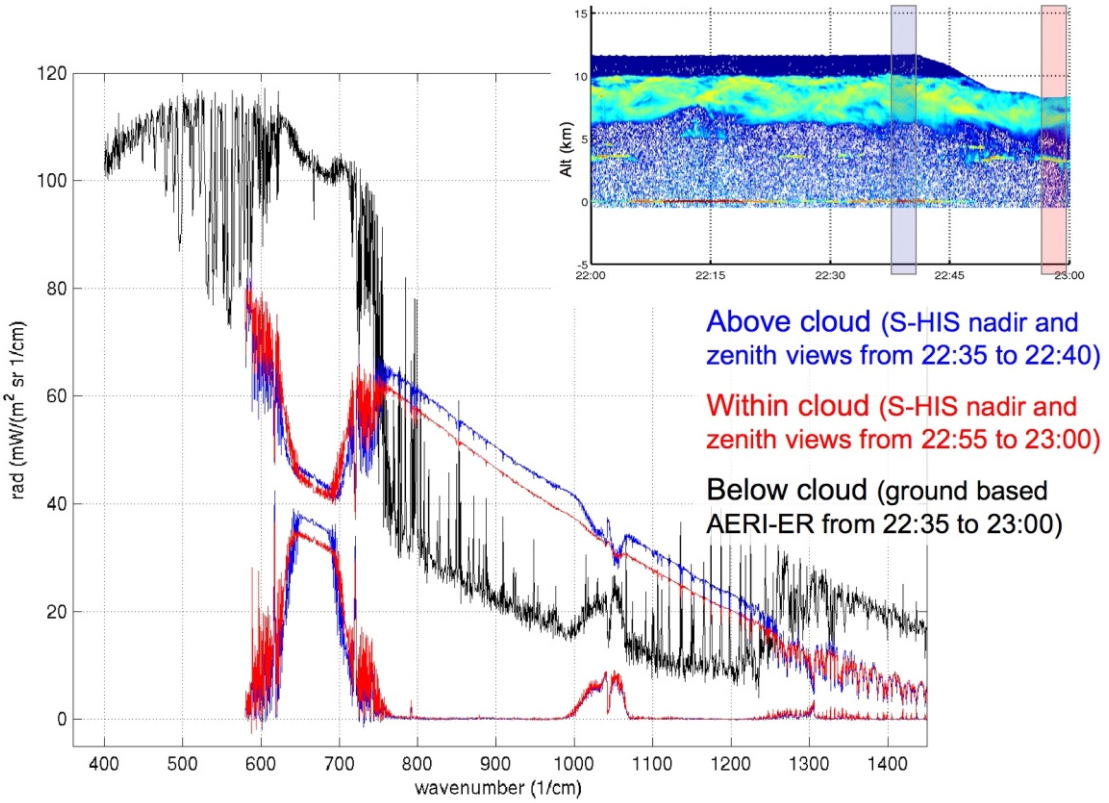

Figure 14: Ground-based AERI-ER and Scanning-HIS measurements (up and down from a 9 and 12 km flight altitude) at Barrow, AK on 17 October 2004. The cloud boundary inset is based on the Proteus cloud detection lidar backscatter data.

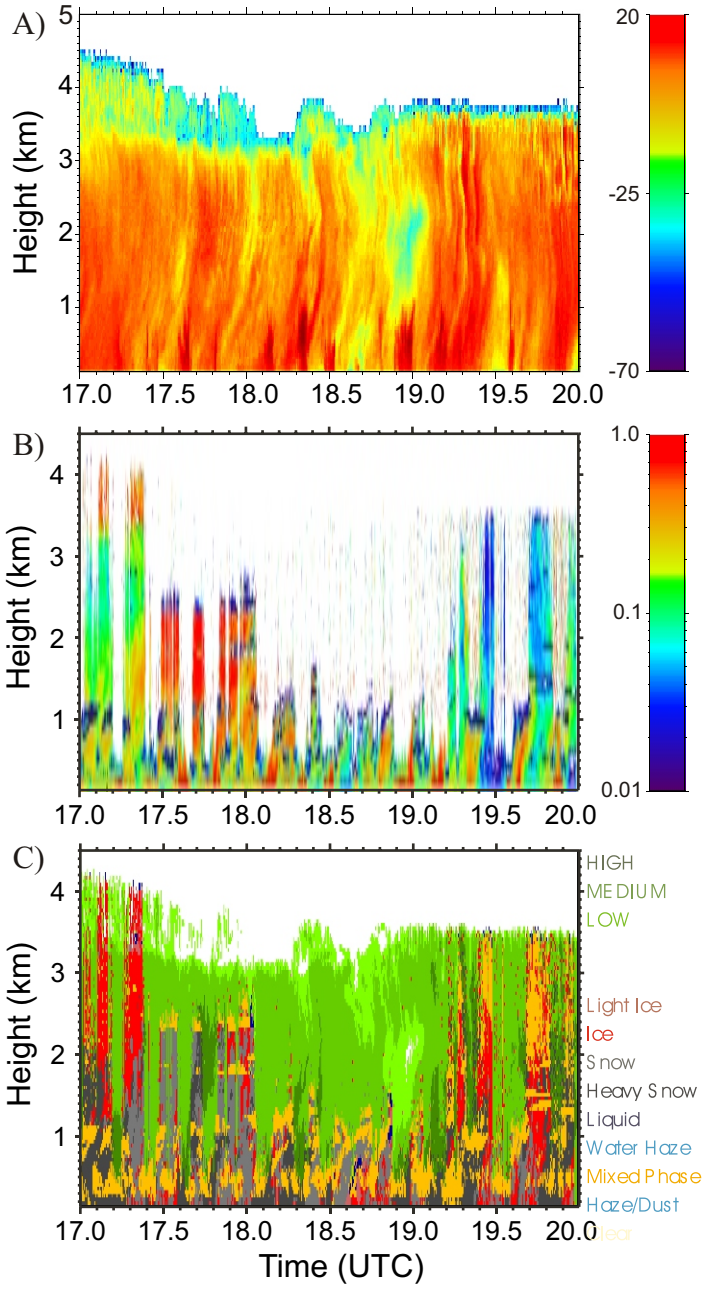

Figure 15: a) MMCR radar reflectivity (top), b) lidar backscatter (middle) and c) radar/lidar cloud phase mask for the UND Citation flight over Barrow on 6 October 2004.

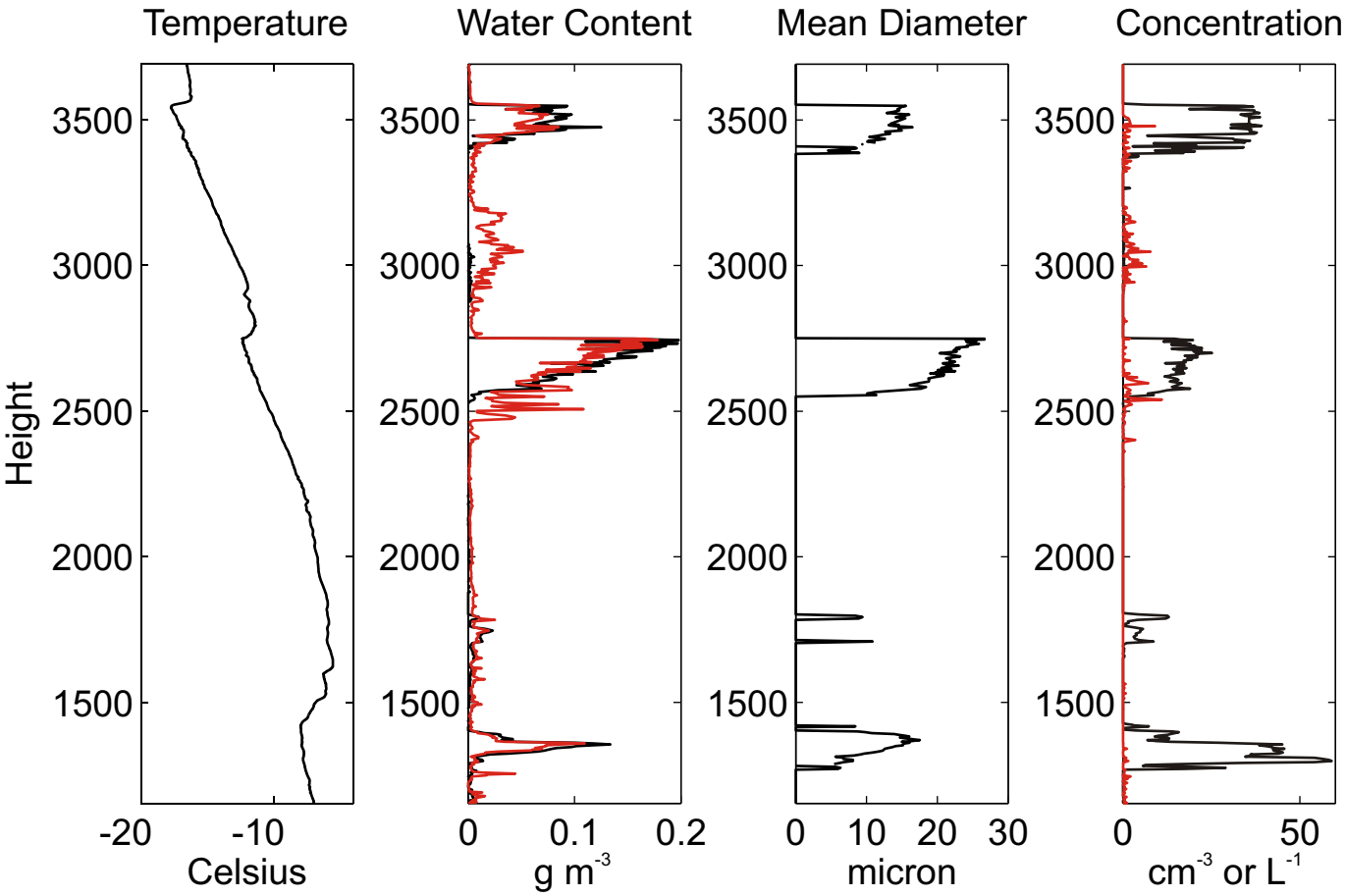

Figure 16: Same as Figure 8, but for 6 October 2004.

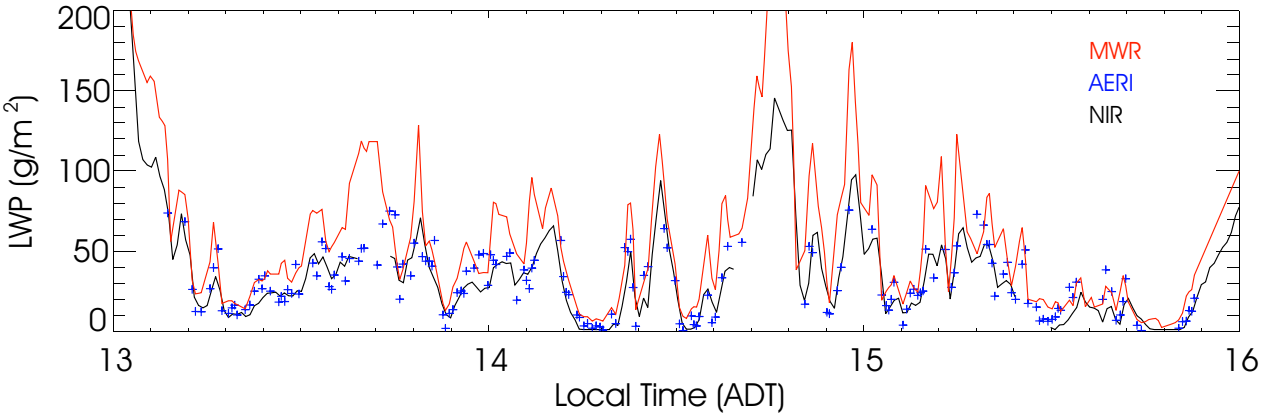

Figure 17: Comparison between three liquid water content retrieval algorithms relying on different parts of the electromagnetic spectrum: microwaves (red line, MWR), infrared bands (blue, AERI) and near-infrared bands (black, near infrared spectrometer).

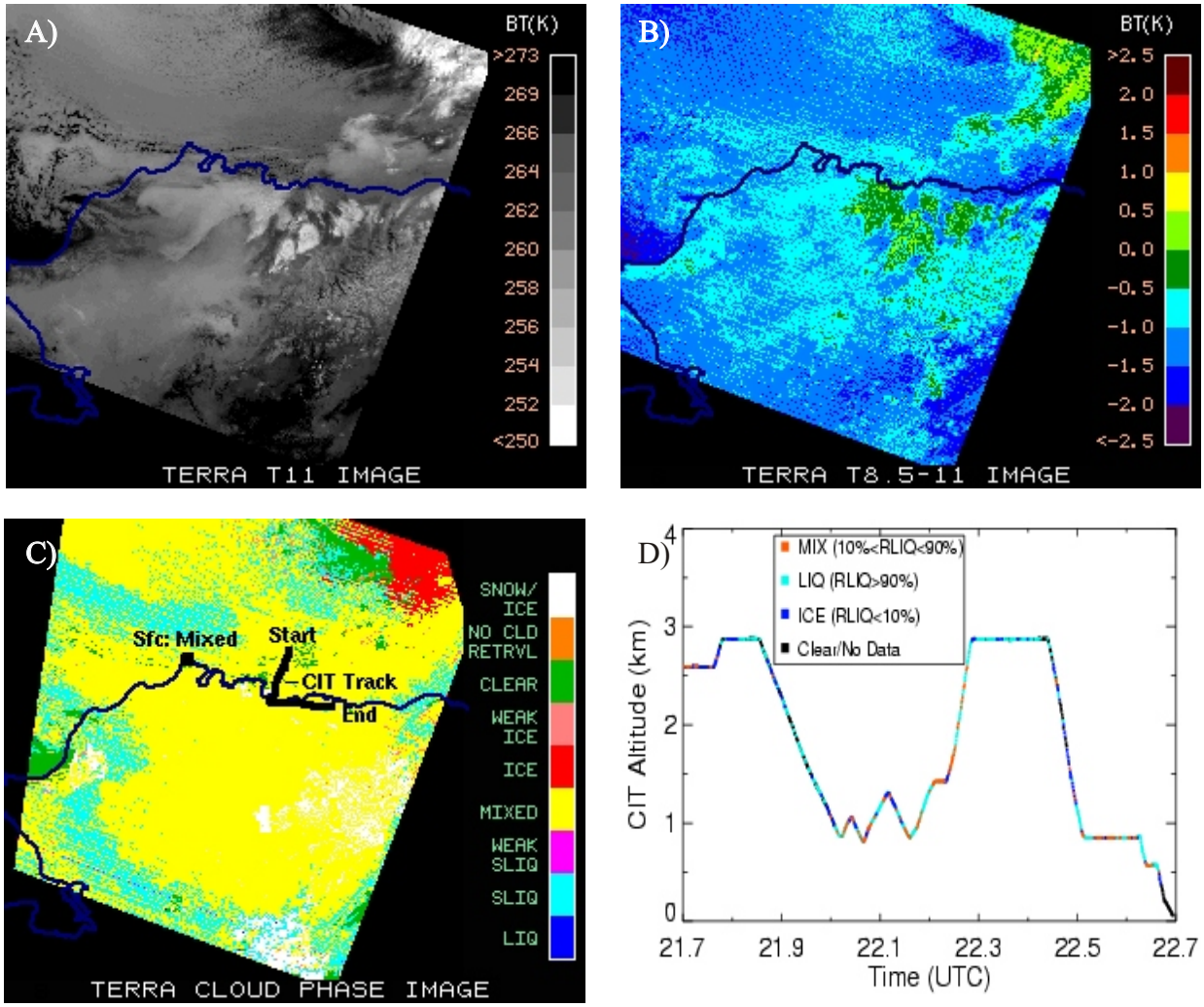

Figure 18: Terra-MODIS imagery and in-situ cloud phase determination from the UND Citation for 22:10 UTC 8 Oct 2004. (a) 11 mm brightness temperature, (b) brightness temperature difference between 8.5 and 11 mm, (c) cloud phase mask, with Citation flight track and surface based phase retrieval, and (d) Citation cloud phase. The surface-based phase retrieval and CIT flight track are also plotted in (c). The LIQ and SLIQ terms in (c) represent liquid and supercooled liquid water, respectively.

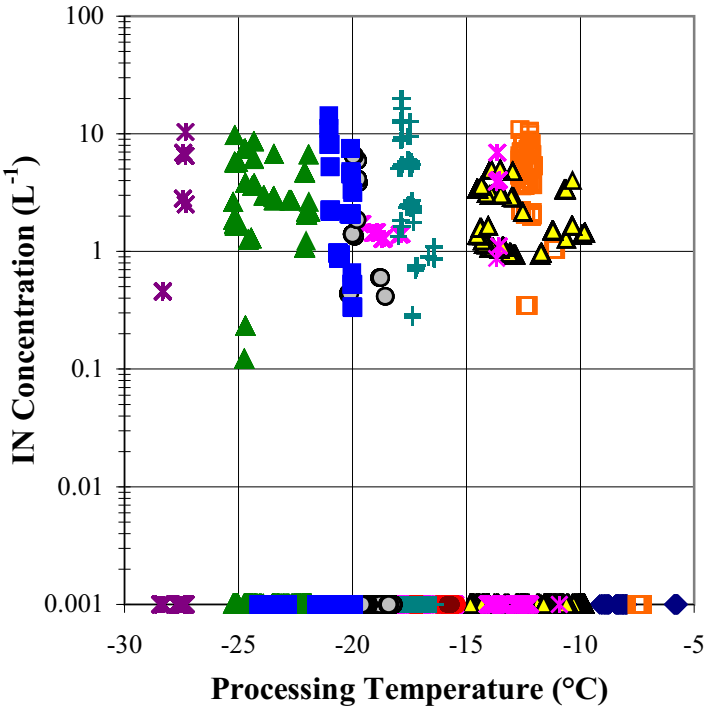

Figure 19: Ice nuclei concentration (60 s average, and corrected to STP) as a function of CFDC processing temperature. Data are limited to measurements for which processing humidity was greater than water saturation, in order to capture deposition, immersion, and condensation freezing nuclei. Individual flights are delineated by symbol. IN concentrations plotted at 0.001 L^{-1} were below background levels, and constituted 85% of the measurements. Thus, while many of the IN measurements shown fall between 1 L^{-1} and 10 L^{-1}, project average IN concentrations were generally below 1 L^{-1}.